Submitted to *Chemosphere*

February 18th, 2019

Revision submitted on May 25, 2019

Dissolution of radioactive, cesium-rich microparticles released from the Fukushima Daiichi Nuclear Power Plant in simulated lung fluid, pure-water, and seawater

Mizuki Suetake,[1] Yuriko Nakano,[1] Genki Furuki,[1] Ryohei Ikehara,[1] Tatsuki Komiya,[1] Eitaro Kurihara[1] Kazuya Morooka,[1] Shinya Yamasaki,[2] Toshihiko Ohnuki,[3] Kenji Horie,[4,5] Mami Takehara[4], Gareth T. W. Law, [6] William Bower,[6] Bernd Grambow,[7] Rodney C. Ewing,[8] and Satoshi Utsunomiya,[1*]

[1]Department of Chemistry, Kyushu University, 744 Motooka, Nishi-ku, Fukuoka 819-0395, Japan

[2]Faculty of Pure and Applied Sciences and Center for Research in Isotopes and Environmental Dynamics, University of Tsukuba, 1-1-1 Tennodai, Tsukuba, Ibaraki 305-8577 Japan

[3]Laboratory for Advanced Nuclear Energy, Institute of Innovative Research, Tokyo Institute of

Technology, 2-12-1 Ookayama, Meguro-ku, Tokyo 152-8550, Japan

[4]National Institute of Polar Research, 10-3, Midori-cho, Tachikawa-shi, Tokyo, 190-8518, Japan

[5]Department of Polar Science, The Graduate University for Advanced Studies (SOKENDAI), Shonan Village, Hayama, Kanagawa, 240-0193, Japan

[6] Radiochemistry Unit, Department of Chemistry, The University of Helsinki, Helsinki Finland, 00014

[7]SUBATECH, IMT Atlantique, CNRS-IN2P3, the University of Nantes, Nantes 44307, France

[8]Department of Geological Sciences and Center for International Security and Cooperation, Stanford University, Stanford, CA 94305-2115 USA

*Correspondence: utsunomiya.satoshi.998@m.kyushu-u.ac.jp

Abstract

To understand the chemical durability of highly radioactive cesium-rich microparticles (CsMPs) released from the Fukushima Daiichi Nuclear Power Plant in March, 2011, we have, for the first time, performed systematic dissolution experiments with CsMPs isolated from Fukushima soils (one sample with 108 Bq and one sample with 57.8 Bq of ^{137}Cs) using three types of solutions: simulated lung fluid, ultrapure water, and artificial sea water, at 25 and 37 ℃ for 1–63 days. The ^{137}Cs was released rapidly within three days and then steady-state dissolution was achieved for each solution type. The steady-state ^{137}Cs release rate at 25 ℃ was determined to be 1.3×10^{3}, 1.3×10^{3}, and 4.7×10^{3} Bq·m^{-2}·s^{-1} for simulated lung fluid, ultrapure water, and artificial sea water, respectively. This indicates that the simulated lung fluid promotes the dissolution of CsMPs. The dissolution of CsMPs is similar to that of Si-based glass and is affected by the surface moisture conditions. In addition, the Cs release from the CsMPs is constrained by the rate-limiting dissolution of silicate matrix. Based on our results, CsMPs with ~2 Bq, which can be potentially inhaled and deposited in the alveolar region, are completely dissolved after >35 years. Further, CsMPs could remain in the environment for several decades; as such, CsMPs are important factors contributing to the long-term impacts of radioactive Cs in the environment.

1. Introduction

In March 2011, ~10^{16} Bq of radioactive Cs was released from the Fukushima Daiichi Nuclear Power Plant (FDNPP) (Buesseler et al., 2017; Stohl et al., 2012), and the surface environment remains contaminated today, mainly with radioactive ^{134}Cs (half-life of 2.1 y) and ^{137}Cs (half-life of 30 y) (Kaneko et al., 2015; Yamasaki et al., 2016). The Cs speciation at the time of release from the reactors was either as a soluble form (*e.g.*, CsOH and CsCl) or as sparingly soluble microparticles enriched in Cs (Adachi et al., 2013). These Cs-rich microparticles (CsMPs) constitute a condensed-matter material that formed during meltdown inside the reactors (Furuki et al., 2017; Imoto et al., 2017a). In general, CsMPs are composed mainly of O, Si, Fe, Zn, and Cs. High-resolution transmission electron microscopy (HRTEM) analysis revealed that SiO_2-glass-matrix-encapsulated Fe-Zn-oxide nanoparticles that adsorb Cs and other fissionogenic products (Furuki et al., 2017; Imoto et al., 2017a, 2017b). Particle sizes range from sub-micron to a few μm in diameter. The Cs concentration in the particles is as high as 8 to 46 wt.% and the radioactivity per unit mass is typically ~10^{11} Bq·g^{-1} (Ikehara et al., 2018). Recent work has shown that CsMPs account for a significant amount of Cs in soils close to FDNPP, and that there are up to ~300 CsMPs per gram of soil (Ikehara et al., 2018).

Because of the high local β and γ radiation, there have been concerns about adverse health effects stemming from inhalation of these particles (Imoto et al., 2017a), since no published data are available for the dose conversion coefficient for the sparingly soluble microparticles with high-density

71 radioactivity (ICRP, 2012, 1993). In addition, a recent study reported the association of discrete debris
72 fragments with CsMPs (Ochiai et al., 2018). The debris fragments contain intrinsic uranium dioxides
73 within Fe-oxides, that also contain other fission products such as Mo and Tc. As such, inhalation of
74 these materials gives a possibility of internal dose by alpha radiation. On the other hand, it is well
75 known that the plume containing CsMPs spread to the Kanto region, including the metropolitan city
76 of Tokyo located ~230 km south of the FDNPP (Adachi et al., 2013; Imoto et al., 2017a; Tanaka et al.,
77 2013). Compared with the CsMPs found near FDNPP, the radioactivity of the individual CsMP
78 characterized in the city of Tokyo, was much lower (0.094–2.3 Bq), indicating that the CsMPs
79 transported across longer distances were generally small, < a few micron in size (Imoto et al., 2017a).
80 Originally, CsMPs were reported to be insoluble in water (Adachi et al., 2013). Considering
81 the properties of CsMPs which have a glassy matrix, they may yet dissolve in ambient conditions;
82 however, knowledge on their dissolution behavior and residence time has been limited to a recent
83 study that reported the dissolution in pure water and seawater (Okumura et al., 2019). The present
84 study demonstrates dissolution experiments involving CsMPs in simulated lung fluid to better
85 understand the mechanisms and kinetics of CsMP dissolution, the residence time, and Cs leaching in
86 human lungs. Additional experimental conditions are tested in ultrapure water and seawater to
87 investigate the CsMP dissolution in the ambient environment
88

2. Methods

2.1. Isolation of Cs-rich microparticles and particle preparation for dissolution experiments

CsMPs with high radioactivity, >100 Bq, are rarely found in Fukushima soil samples; however, highly radioactive CsMPs were necessary for the dissolution experiments presented here in order to permit direct determination of Cs radioactivity leached into solution. Two such particles (>100 Bq) were successfully prepared in the present study. The CsMPs were isolated from surface soils collected from Ottozawa and Koirino, Okuma town in the Fukushima prefecture. Both sites are within 5 km of FDNPP. The soil samples were labeled KU-312 and -150, respectively, in the Kyushu University Fukushima sample archive. However, within the present article, the isolated CsMPs are labeled OTZ and KOI, which, to avoid confusion, differ from the labels used in our previous studies (Furuki et al., 2017; Imoto et al., 2017b; Ochiai et al., 2018). Isolation of the CsMPs followed the procedure described in our previous study (Furuki et al., 2017). First, the soil samples were sieved through a 114-μm mesh. The samples were dispersed on an Al board and covered with a plastic sheet; an imaging plate (IP, Fuji film, BAS-SR 2025) was then placed on the samples for 5−25 minutes. The autoradiograph image was recorded with a pixel size of 100 μm using an IP reader (GE, Typhoon FLA 5100). After identifying the positions of intense radioactive spots, droplets of pure water were added to the positions and then taken up using a pipet to make a suspension with a small amount of soil particles. During this procedure, the sample was wet for a limited time compared to the duration of

107 the dissolution experiments. The procedure was repeated until the suspension did not contain a
108 significant amount of soil particles. Subsequently, the position containing a highly radioactive spot
109 was sampled using double-sided adhesive carbon tape (Nissin EM Inc.) for scanning electron
110 microscopy. The piece of carbon tape with the radioactive particle was cut into smaller pieces using a
111 blade.

112 After isolation, each CsMP was adhered to the surface of double-sided adhesive carbon tape
113 with the dimension of ~50×50 μm and then fixed to a 1×1 cm^2 Al plate. Given the size of the CsMPs,
114 this method was necessary to fix the CsMPs in place during our dissolution method (see below). A
115 caveat of this method is that the fraction of each CsMP attached to the carbon tape would likely
116 experience lower rates dissolution. Unfortunately, the difficulty of obtaining and extracting CsMP
117 samples, and the complexity of completing dissolution experiments with single particles of <6 μm
118 diameter, makes this caveat unavoidable. However, the dissolution rates presented herein is within the
119 same order of magnitude of results that could be obtained if experiments were completed without
120 CsMP adhesion. Also, of note, the CsMPs used in the study were not carbon-coated, even for scanning
121 electron microscopy (SEM) observations.

122 After isolation of each CsMP, some soil particles, including clays, remained, surrounding
123 the CsMP on the carbon tape (see Fig. 1a for case of KOI and Fig. S1 for the case of OTZ). To prevent
124 reactions between the remaining clays and the dissolved Cs ions, or dissociation of Cs previously

adsorbed to the clays, the entire surface of the specimen (except the CsMP) was coated with tungsten (W) by using a focused-ion-beam system (Quanta 3D 200i, FEI). The result of this procedure was that only the CsMP surface was in contact with the solution because it was not coated by W. Further, during the W treatment on the surrounding soil particles, observation with the ion-beam in the FIB was minimized to maintain the CsMP surface as undamaged due to the absence of W coat. To test the efficiency of this W-coating strategy, a dissolution experiment was conducted on a specimen (prepared in the same way) with no CsMP. The gamma spectrum revealed no peak at the position of ^{137}Cs, confirming that the W-coated soil particles were not reactive in the experiments (Fig. S2). In addition, the potential for re-adsorption of Cs onto double-sided adhesive carbon tape and Al plate was investigated. We prepared the same material without any CsMPs; that is, a small piece of double-sided adhesive carbon tape on Al plate. The material was immersed in 5 ml of the simulated body fluid with 1.79±0.01 Bq of ^{137}Cs for 6 days at 25 ℃. After immersion, the radioactivity of ^{137}Cs of the solution was measured as 1.78±0.02 Bq, indicating that no Cs adsorbed to the double-sided adhesive carbon tape and Al plate. As such, it is highly unlikely that there would have been any re-adsorption of the radioactive Cs leached from the CsMP during the dissolution experiment.

2.2. Dissolution experiment with Cs-rich microparticles

The CsMPs used in the present experiment were isolated from the natural environment one

143 (KOI) and six years (OTZ) after deposition from the FDNPP. As such, they would have already
144 experienced some degree of post depositional alteration under wet and dry conditions. This cannot be
145 quantified.

146 In our dissolution experiment approach, each prepared CsMP (see section 2.1) was statically
147 immersed in a 5.0 mL solution (see below for solution types and the immersion sequence for each
148 CsMP) in a 10 mL Perfluoroalkoxy alkane (PFA) vessel sealed with a screwed lid to avoid evaporation.

149 In order to simulate the possible conditions of exposure for CsMPs after deposition in the
150 natural environment, which could include either wet, or wet/dry cycles, two types of immersion
151 conditions were prepared in the dissolution experiments: (i) wet and dry, and (ii) wet only. The
152 conditions are summarized in Fig. 2a. For condition (i), the CsMP being studied was immersed in an
153 aliquot of solution, reacted, and then removed from the solution after an arbitrary period. Next, the
154 solution was analyzed using gamma spectrometry. The CsMP was left to dry in air during the gamma
155 measurements, which typically lasted for 1–7 days depending on counting statistics. After counting,
156 the CsMP was then immersed again in the same solution to continue the dissolution processes for the
157 desired time. This process was repeated until the end of the reaction period. For condition (ii), the
158 CsMP being studied was immersed in an aliquot of solution and removed after a certain time. The
159 CsMP was then quickly immersed in ultra-pure water (UPW) to maintain its wet surface and also to
160 rinse the surface. Soon thereafter, the CsMP was immersed in another aliquot of solution, which had

161 the same initial composition as the previously used solution, but without any leached Cs. The solutions
162 after the reactions of all durations were analyzed by gamma spectrometry.

163 The sequence of immersion for each particle is summarized in Fig. 2b. The KOI CsMP was
164 first immersed and reacted in simulated lung fluid (SLF) (Marques et al., 2011) at 25 ℃ for 31 days,
165 with occasional solution sampling completed under wet and dry conditions (i.e. condition (i); Fig. 2a;
166 Seq. 1). The composition of the SLF is given in Table S1. After reaction in the SLF, the same CsMP
167 was then immersed in the ultra pure water (UPW; 18.2 MΩcm) and reacted at 25 ℃ for 43 days as a
168 control experiment (Seq. 2), with occasional solution sampling taking place under condition (i). After
169 reaction in the UPW, the CsMP was immersed in SLF again, but at 37 ℃ for 63 days (Seq. 3), with
170 occasional solution sampling under condition (i). After reaction, the CsMP was rinsed with UPW,
171 because secondary phase precipitation was observed over the sample. The rinsing process efficiently
172 removed the precipitates. The same CsMP was then immersed in artifical seawater (ASW) purchased
173 from Daigo Inc. at 25 ℃ for 30 days (Seq. 4), with occasional solution sampling under condition (i).
174 Table S1 gives the composition of the ASW. Finally, the CsMP was immersed in SLF at 25 ℃ for 30
175 days (Seq. 5), with occasional solution sampling under the wet only condition (i.e. condition (ii); Fig.
176 2a). The UPW, ASW, and SLF had a pH of 7.0, 7.8, and 7.4, respectively, as measured by using a
177 TOKO TPX-999i pH meter (PCE108CW-SR) equipped with an calibrated electrode (PCE108CW-SR).

178 The OTZ CsMP was immersed (Fig. 2b) in UPW at 25 ℃ for 30 days (Seq. 1), with

179 occasional solution sampling under condition (i). Then, the OTZ CsMP was immersed in SLF at 25 ℃
180 for 10 days (Seq. 2), with occasional solution sampling under condition (i).
181 The SLF after the experiments was further used for an evaporation test; here, the SLFs for
182 KOI (from the initial SLF treatment) and OTZ CsMPs were condensed at 15 and 9.1 times by
183 evaporating under air, respectively. The pH of the condensed SLF droplets of ~0.3 ml was measured
184 by using a compact pH meter (LAQUAtwin-pH-22B; HORIBA).
185
186 **2.3. Scanning electron microscopy**
187 Secondary-electron images and the elemental maps were obtained by using SEM
188 (Shimadzu, SS-550) equipped with energy dispersive X-ray analysis (EDX, EDAX). The
189 acceleration voltage was 15–25 kV.
190
191 **2.4. Gamma spectrometry**
192 The radioactivity of ^{134}Cs and ^{137}Cs in the CsMPs was determined by using gamma
193 spectrometry. The point-source standard prepared in our previous study (Furuki et al., 2017) was
194 used for calibration to analyze the microparticles. The Cs radioactivity of the solutions in sealed
195 Teflon vessels was also measured after reactions. To calibrate the gamma spectrum for the solution
196 sample, 5 mL of the solution with a known concentration of radioactive Cs in a PFA vessel of the

197 same shape was measured and used as the standard. The radioactivity measurements were made by
198 using germanium semiconductor detectors GMX23 and GMX40 (all from SEIKO E&G) at the
199 Center for Radioisotopes of Kyushu University. The acquisition time ranged from 1 to 162 hours so
200 that the net area of the ^{134}Cs and ^{137}Cs peaks both exceeded 1000 counts. Reaching over 1000 counts
201 results in a relative uncertainty better than 3%. The errors in gamma measurements were calculated
202 in Gamma Studio (SEIKO EG&G).
203
204 **3. Results and Discussion**
205 **3.1. Properties of CsMPs used in dissolution experiment**
206 The radioactivity and the associated parameters of the two CsMPs; KOI and OTZ, prior to
207 the dissolution experiments, are summarized in Table 1. The ratio of the radioactivity of ^{134}Cs to that
208 of ^{137}Cs, decay-corrected to March 12, 2011, is ~1, indicating that the CsMPs originated from FDNPP.
209 The experimental results reported hereinafter are based only on non-decay-corrected ^{137}Cs, because
210 its radioactive decay is negligible due to its half-life of 30 years being much longer than the duration
211 of the experiments.
212 Figure 1 shows the SEM images and the elemental maps of the major constituents. The
213 particle size is 5.64 μm for KOI and 4.20 μm for OTZ. The elemental distribution of major constituents
214 within the CsMPs appears to be same as that of CsMPs in previous studies, which include examples

215 of CsMPs transported over large distances from the FDNPP (Adachi et al., 2013; Furuki et al., 2017;
216 Imoto et al., 2017a, 2017b; Yamaguchi et al., 2016).
217
218 **3.2. Dissolution experiments with CsMPs**
219 Figure 3 shows the time course of ^{137}Cs radioactivity release during the dissolution
220 experiments with KOI from seq. 1 to seq. 5. The measured radioactivities are also given in Table 2. In
221 the present experiment, the radioactive Cs leached from the CsMP was successfully determined using
222 gamma spectrometry despite the extremely low concentrations. The maximum radioactivity of ^{137}Cs
223 ~2 Bq in 5 ml solution is equivalent to only ~9×10^{-13} mol/L. This low concentration of Cs is negligible
224 in evaluating the effects on the solution chemistry. Based on the composition of CsMP (Furuki et al.,
225 2017), it is likely that the amount of the other major constituents (Si, Fe, and Zn) that leached from
226 the CsMP were very low.
227 In seq. 1 – 3, the ^{137}Cs radioactivity rapidly increase after immersing the CsMP, and then
228 reaches steady state after 3 days. We calculate the ^{137}Cs release rate after the release rate attains an
229 apparent steady state, meaning that the radioactivity data can be approximated by a regression line.
230 For the SLF at 37 ℃ (seq. 3) the Cs release did not reach a clear steady state, as the data after 63 days
231 deviates lower than the linear trend (Fig. 3), which likely is due to precipitation of secondary phases
232 observed after 63 days at 37 ℃. For experiments at 25 ℃ (seq. 1, 2, and 4) under condition (i), the

233 ^{137}Cs release rate is calculated to be 4.68×10^3, 1.33×10^3, and 1.29×10^3 Bq·m^{-2}·s^{-1} for SLF, UPW, and

234 ASW, respectively. The release rate in the SLF is clearly greater than that in UPW (by a factor of 3.5).

235 Based on the ^{137}Cs release rate, we calculate the radioactivity over time due to the dissolution of CsMP

236 by using

237 $$D_{t,x} = \left\{D_{0,137} - 4\pi k \int_0^t \left(r_0 - \frac{k}{d}t\right)^2 dt\right\} \times e^{\left(-t\times ln2/\tau_{1/2,x}\right)}$$

238 $$= \left\{D_{0,137} - 4\pi k \left(r_0^2 t - \frac{kr_0}{d}t^2 + \frac{k^2}{3d^2}t^3\right)\right\} \times e^{\left(-t\times ln2/\tau_{1/2,x}\right)}$$

239 (1)

240

241 where $D_{t,x}$ and $D_{0,x}$ are the ^{x}Cs radioactivity of the CsMP at time t and time zero in Bq. The x denotes

242 the mass of the Cs isotope: 134 or 137, r_0 is the radius of CsMP at time zero (time is in units of minutes),

243 k is the ^{137}Cs radioactivity leach rate determined based on the ^{137}Cs release per unit area of CsMP

244 (Bq·m^{-2}·s^{-1}), d is the radioactivity per unit volume of CsMP (Bq·m^{-3}), and $\tau_{1/2,x}$ is the half-life of ^{x}Cs

245 (seconds). In this dissolution model, the CsMP was approximated as a sphere and the decreasing rate

246 of radius was assumed to be constant, which was calculated based on the ^{137}Cs leach rate. This model

247 accounts for the decrease in the surface area of the CsMP as a function of time.

248 Based on the release rate of ^{137}Cs, the duration for the complete dissolution (t_{total}) and for

249 dissolution to particle sizes less than 100 nm (t_{100nm}) were calculated for all conditions (Table 3).

250 Because the solubility of particles of size less than 100 nm is greater than that of the bulk sample

251 (Stumm, 1992), the dissolution rate after reaching t_{100nm} can be greater for these particles, and actual
252 total time can be less than t_{total}. In this calculation, t_{total} was calculated based on the equation (1); thus,
253 the actual total time may be plotted between t_{100nm} and t_{total}. The estimated time course of radioactivity
254 is calculated for all conditions based on the ^{137}Cs release rate, and the results are shown in Fig. 4.
255 Under condition (ii), the ^{137}Cs release rate from the KOI CsMP was 1.5×10^{3} Bq·m^{-2}·s^{-1} in
256 SLF (Fig. 3). The release rate is only one third of that for condition (i) (wet and dry), which clearly
257 indicates that the wet condition on the CsMP surface is a critical factor in addition to the sequence of
258 the alteration. There was no visible secondary precipitates over the CsMP surface. The effects of the
259 drying surface can be explained by the increasing solute concentration due to the evaporation of the
260 water layer on the CsMP surface. For the SLF, pH change upon evaporation was also possible. Thus,
261 the SLF after the experiments (seq. 1 in case of KOI) was further used for the evaporation test, in
262 which the SLFs for KOI and OTZ were condensed at 15 and 9.1 times by evaporation under air,
263 respectively. The pHs of SLF for KOI and OTZ changed from 7.4 to 5.7 and 5.9, respectively. Thus,
264 the further condensation of water results in lower pH conditions in the SLF under condition (i). The
265 lowered pH in the condensed SLF is most likely the major factor accelerating the dissolution rate;
266 indeed, several previous studies have reported faster dissolution at acid pH as well as alkaline pH
267 (Abraitis et al., 2000; Gislason and Oelkers, 2003a). In addition to the pH decrease, the evaporation
268 increases the ionic strength, which can affect the dissolution rate by influencing the surface potential

(Icenhower and Dove, 2000; Vogelsberger et al., 1999). However, the dissolution in ASW is no faster than that in UPW, indicating that the ionic strength has little effect on the dissolution rate. Indeed, previous studies have pointed out minimal effects of ionic strength on glass dissolution in the case of saline brines (Braithwaite, 1980; Grambow, 1990). Thus, the slow dissolution under condition (ii) without evaporation can be explained by pH decrease due to the evaporation. Rapid initial release of Cs was also recognized in the sequence 1 – 3. There are some factors that can potentially cause this rapid release, such as cation exchange at initial stage of glass dissolution; however, the most plausible reason in the case of this experiment was sample treatment before starting the sequence as revealed in Fig. 3. Here, the CsMP was dried after seq. 1 and 2 followed by the immediate use in the subsequent experiment, whilst the CsMP was thoroughly rinsed after seq. 3. Thus, relatively high concentrations of Cs that remained on the dried surface likely account for the rapid increase at the initial stage.

For the OTZ sample, the ^{137}Cs release rate R_{Cs}, at 25 °C, was determined to be 5.5×10^{2} Bq m^{-2} s^{-1} for UPW, while the Cs release did not reach the steady state in case of SLF after 10 days. Thus, only the maximum dissolution rate was estimated for SLF; $<1.0\times10^{3}$ Bq·m^{-2}·s^{-1} (Fig. 5, Table 2). Dissolution in SLF can be accelerated compared with that in UPW due to the effects of organic matter and other ions in the SLF, since previous studies have reported that silica dissolution is enhanced by organic matter through the formation of carboxylate-Si complexes and the nucleophilic attack onto the Si in the Si–O network (Braun et al., 2016; McMahon et al., 1995). The time course of radioactivity

287 calculated for OTZ based on the ^{137}Cs release rate is plotted in Fig. 6.

288 Note also that secondary phases precipitated onto the surface of OTZ after 10 days in SLF,
289 whereas such precipitates were scarcely present in the dissolution experiment of KOI up to 30 days.
290 The precipitates were characterized by SEM-EDX to be mainly Ca phosphate (Fig. 7). The
291 precipitation of Ca phosphate is consistent with the results of calculation for the saturation index of
292 the SLF solution using the thermodynamic calculation code, the Geochemist's workbench version 7
293 and the thermodynamic database of thermo.com.v8.r6+ (Table S2). Thermodynamically, the initial
294 SLF solution is supersaturated with respect to hydroxylapatite and whitlockite. As described above,
295 the amounts of leached constituents from the CsMP are extremely low, in the order of 10^{-13} – 10^{-12}
296 mol/L. Hence, the effects on the ionic strength and saturation index of the solution are negligible in
297 the present experiment; that is, intrinsic Cs phase cannot precipitate on the surface during the
298 dissolution experiment.

299 Regarding the timing of Ca phosphate formation, OTZ should contain a higher Si
300 concentration, because CsMP with low Cs content typically contains high Si content (Furuki et al.,
301 2017). The difference in timing of phosphate formation may be attributed to the different amount of
302 SiO_2 gel layer, as a previous study suggested that the hydrate silica provides favorable sites for the
303 apatite nucleation (Ohtsuki et al., 1992). In the present study, the dissolution experiment was stopped
304 at the onset of precipitation so that the dissolution rate was not significantly affected by the reaction

progress for either KOI or OTZ. Experiments for longer periods than reported herein would likely lead to complete coverage of the CsMP surface with Ca phosphate. Such a process is highly probable in an actual alveolar region, depending on the flow-rate of fluid in contact with the CsMP. The Ca-phosphate coating may serve as a passive layer, leading to a slower dissolution rate as compared with that determined in the present study. Indeed, a previous study reports that the formation of a Ca-phosphate coating slowed the dissolution of core materials in simulated body fluid (Cabrini et al., 1997; Wen et al., 2009).

3.3. Possible mechanisms of CsMP dissolution

Table 3 summarizes the ^{137}Cs release rates for all conditions. First, we assume the simplified model; a constant Cs/Si concentration ratio in the glass as well as congruent dissolution at the scale of the present experiment. Then, the rates can be converted to Si release rates,

$$R_{Si} = R_{Cs} \times (M_{Cs2O} / M_{SiO2}) \times (W_{SiO2} / W_{Cs2O}) / 2, \quad (2)$$

where R_i is the release rate of ^{137}Cs or Si (mol m^{-2} d^{-1}), M_i is the molecular weight, and W_i is the mass fraction of species i (wt.%). Dividing the release rate of Cs in $Bq \cdot m^{-2} \cdot d^{-1}$ by the Cs inventory in the glass in $Bq \cdot g^{-1}$ and assuming homogeneous distribution of Cs in the glass gives overall glass dissolution rates in $g \cdot m^{-2} \cdot d^{-1}$. The composition of OTZ is required for the conversion; however, the composition of OTZ was difficult to determine precisely using SEM-EDX because of the X-ray signals

323 emitted from the surrounding particles and the Al substrate. Thus, the composition of OTZ is assumed
324 to be similar to that of the other CsMP, which has a similar radioactivity. OTZ22 (KU archive label)
325 is the other CsMP, which contains 65 wt.% SiO_2, 13 wt.% Cs_2O, and 7.9 wt.% ZnO. (See Table S3 for
326 a full list of chemical compositions determined by TEM-EDX and the radioactivity with the associated
327 parameters. Figure S4 provides further TEM results). OTZ22 has a radioactivity per unit mass
328 (3.38×10^{11} Bq·g^{-1}) similar to that of OTZ (3.15×10^{11} Bq·g^{-1}) (Table 1). Note that the conversion from
329 Bq·g^{-1} to Cs wt% was not straightforward because of unknown composition of the other Cs isotopes.
330 The inner structure of CsMP generally exhibits numerous heterogeneities, such as nanoscale
331 inclusions of various fission products and pores (Furuki et al., 2017). The nanoscale texture inside
332 CsMPs is schematically illustrated in Fig. 8. In most cases, Cs is distributed by association with Fe-
333 Zn-oxide nanoparticles (Furuki et al., 2017; Imoto et al., 2017a). The high radioactivity per unit mass
334 such as in KOI is generally ascribed to intrinsic Cs-nanoparticle inclusions. These nanoparticles
335 become embedded in the SiO_2 glass matrix. In these models, the Cs initially exposed to the surface of
336 the CsMP rapidly dissolves, and the Cs inside the particle is released as the surrounding SiO_2 glass
337 matrix dissolves, which proceeds through hydrolysis of Si–O–Si bonds (Xiao and Lasaga, 1994). The
338 hydrolysis of Si-O bonds is expected to be the rate-limiting process in this case. At high concentrations
339 of dissolved orthosilicic acid in solution, glass dissolution rates are expected to drop (Grambow, 2011);
340 however, such conditions are not expected in the present experiments. The dissolution properties of

341 the other constituents of CsMP, Fe-Zn-oxide nanoparticles, are unknown, although the dissolution of
342 the SiO_2 glass matrix is expected to release nanoparticles associated with Cs. A previous study reported
343 that Cs leaching from CsMP may occur at acidic pH (Yamaguchi et al., 2016). Although glass
344 dissolution proceeds by cation release at low pH, a previous study reported a congruent dissolution at
345 high pH (Abraitis et al., 2000). In the present study, the Cs leach rate is constrained by the dissolution
346 of SiO_2 glass matrix, which allows to approximate as an apparent congruent dissolution at "macro-
347 scale". Hence, we use equation (2) to deduce the approximate dissolution rate of the microparticle for
348 roughly comparing the order of dissolution rate with that of other glasses. The dissolution rate (i.e.,
349 the Si release rate) is determined to be 1.26×10^{-6} and $<2.39\times10^{-6}$ mol m^{-2} d^{-1} for OTZ immersed in
350 UPW and SLF, respectively. This may be compared with results of dissolution rates of various glasses
351 and the effects of glass composition on glass dissolution rates have been described extensively in the
352 literature (Grambow, 2011). Using the reported linear rate terms and activation energies, we obtain the
353 dissolution rates: 0.036 $g\cdot m^{-2}d^{-1}$ for Corning soda lime glass, 0.016 $g\cdot m^{-2}d^{-1}$ for PPG soda lime glass,
354 1.8×10^{-4} $g\cdot m^{-2}d^{-1}$ for Kimble R6 soda lime glass, and 6×10^{-6} $g\cdot m^{-2}d^{-1}$ for obsidian. Kimble RG soda
355 lime glass has the composition of 74 wt.% SiO_2, 12.9 wt.% Na_2O and 8.3 wt.% CaO, and obsidian has
356 the highest Si concentration (76 wt.%) and the lowest alkali content (8.6 wt.%). Thus, the dissolution
357 rate of the CsMP is close to pure silica glasses or low alkali glasses rather than to that of more complex
358 high alkali glasses. Indeed, the Cs content of the glasses of 13.5 wt.% is rather low compared with that

359 in the above mentioned glasses, if presented in molar fraction. Dissolution of silica glass fibers at
360 37 ℃ in physiological gamble solution gave dissolution rates 1.1 $nm \cdot d^{-1}$ or 4.2×10^{-5} $g \cdot m^{-2} \cdot d^{-1}$ (Scholze,
361 1991). Dissolution rates of SiO_2 (62 wt.%)-Al_2O_3(2-4 wt.%)-B_2O_3(6-8wt.%)-CaO(8 wt.%)-MgO(3.5-
362 4 wt.%)-Na_2O(14-16 wt.%) glasses fibers in physiological solutions at 37 ℃ and pH 7.5 were much
363 higher, varying between 0.03 and 0.18 $g \cdot m^{-2} \cdot d^{-1}$ (Potter and Mattson, 1991). Dissolution rates varied
364 as function of fiber diameter between 2 and 10 μm by as much as 27%. In vivo (rat lung tissue or
365 macrophages) dissolution rates of a glass fiber of similar composition varied between 0.0005 and
366 0.003 $g \cdot m^{-2} \cdot d^{-1}$. For comparison, the dissolution rates of Si-based glasses (Abraitis et al., 2000;
367 Crovisier et al., 1987; Gislason and Oelkers, 2003b; Hamilton et al., 2000; Oelkers and Gislason,
368 2001) and amorphous silica (Icenhower and Dove, 2000; Seidel et al., 1997) at near room temperature
369 (25 ℃) are plotted in Fig. 9. Although the dissolution rate estimated for OTZ is greater than that of
370 amorphous silica, it is within the range of the dissolution rates of Si-based glasses reported in previous
371 studies. Thus, the kinetics of CsMP dissolution is similar to that of glass dissolution. Higher dissolution
372 rates may also be explained by the formation of a Cs silicate glass but we have too little information
373 to forward this interpretation.
374
375 **3.4. Estimation of residence time of inhaled CsMPs**
376 As mentioned in the introduction, the size of CsMPs transported from the FDNPP over long

377 distances were small (< a few μm); however, these CsMPs were mainly comprised of silicate glass, as
378 per the larger CsMPs found closer to the FDNPP. Hence, it is reasonable to assume that the dissolution
379 processes occurring in inhaled CsMPs follow the mechanisms described above. To estimate the
380 residence time and the radioactivity transition of the potentially inhaled CsMPs, we assumed the
381 maximum dissolution rate of OTZ because the Cs concentration (based on the radioactivity per unit
382 mass) of KOI is too high and likely contains inclusions of intrinsic Cs nanoparticles. The maximum
383 release rate of ^{137}Cs, R_{Cs}, for OTZ is normalized based on the ^{137}Cs concentration (mole per m^3 per
384 second). The typical size of the CsMPs ranges from ~0.5 to ~3 μm and the Cs concentration ranges
385 from a few wt.% to ~30 wt.% (Furuki et al., 2017; Ikehara et al., 2018). According to Schlesinger,
386 microparticles in the same size range can potentially deposit in pulmonary region at ~20 – 40 %
387 (Schlesinger, 1989). It is noted that the microparticles are subject to several clearance pathways. Some
388 microparticles can be translocated to the lymphatic system, and the half-time of eliminating the
389 microparticles from lymph nodes was estimated to be tens of years (Roy, 1989).

390 In the following calculation, the size and ^{137}Cs concentration of a CsMP are set to 2 μm and
391 1.09 Bq, respectively, as obtained from a previous study (Imoto et al., 2017a). The isotope ratio of
392 ^{134}Cs to ^{137}Cs is set to 1.0, and we assume that inhalation occurs on March 15, 2011. Consequently,
393 t_{total} and t_{100nm} for the CsMP in the SLF are calculated to be 38.6 and 34.9 year, respectively, for
394 condition (i) (wet and dry), indicating that the CsMPs can persist to the present time (Fig. 10).

The dissolution rate under condition (ii) (wet only) may be a somewhat slower than that under condition (i). Uncertainty in the condition surrounding CsMPs in the alveolar region exists over longer periods. Whether the CsMPs remain in the lung depends on the surrounding aqueous conditions; humid in ordinary case, while often wet in case of pneumonia. In addition, the Ca-phosphate coating should precipitate over the CsMPs and potentially slow the dissolution, which would lead to a longer residence time than that estimated based on the simple dissolution experiments discussed herein. Note also that, when CsMPs contain a high Zn concentration, their dissolution and the precipitation of the Ca-phosphate may be retarded by soluble Zn (Ma et al., 2018). In case of phagocytosis, the pH can be slightly acidic, 4.5, which may promote the dissolution of CsMPs.

4. Conclusions

Based on the present experimental study, we conclude that the CsMPs, which were considered heretofore to be insoluble (Adachi et al., 2013), can dissolve in a manner similar to that of a silicate glass. Although the number of CsMPs in the present dissolution experiments was limited due to the scarcity of highly radioactive CsMPs (>100 Bq), this first experimental study provides crucial insights into the dissolution behavior of CsMPs. Based on the present experiment, the dissolution rate is controlled by various factors, such as (i) the CsMP composition, (ii) the wet and dry condition of the CsMP surface, and (iii) the organic substances in SLF solution. In the present study, the ionic

413 strength of seawater does not significantly affect the dissolution rate. Note also that a passive Ca-
414 phosphate layer may form upon extended contact with SLF, which may decrease the dissolution rate.
415 Consequently, when inhaled, CsMPs as small as ~ 2μm can potentially be deposited in the alveolar
416 region, and these particles are expected to be durable to chemical alterations in SLF for several decades.
417 In addition, CsMPs can potentially remain in various environments beyond several decades, which is
418 consistent with the fact that numerous CsMPs have been discovered under natural weather conditions
419 in the environment seven years after the nuclear disaster. CsMPs are readily transportable in river
420 water and the sedimentation in the ocean is expected to be slow due to their small size (Earle, 2015).
421 Considering the high radioactivity of CsMPs, their migration is one of the key processes governing
422 the dynamics of radioactive Cs in the contaminated environments around Fukushima Daiichi.
423

Acknowledgments

The authors are grateful to Dr. Watanabe for her assistance on SEM analyses at the Center of Advanced Instrumental Analysis, Kyushu University. This study is partially supported by JST Initiatives for Atomic Energy Basic and Generic Strategic Research and by a Grant-in-Aid for Scientific Research (KAKENHI) from the Japan Society for the Promotion of Science (16K12585, 16H04634, No. JP26257402). S.U. is also supported by the Mitsubishi Foundation/Research Grants in the Natural Sciences and by ESPEC Foundation for Global Environment Research and Technology (Charitable Trust) (ESPEC Prize for the Encouragement of Environmental Studies). The findings and conclusions of the authors of this paper do not necessarily state or reflect those of the JST.

436 REFERENCES

437 Abraitis, P.K., Livens, F.R., Monteith, J.E., Small, J.S., Trivedi, D.P., Vaughan, D.J., Wogelius, R.A.,
438 2000. The kinetics and mechanisms of simulated British Magnox waste glass dissolution as a
439 function of pH, silicic acid activity and time in low temperature aqueous systems. Appl.
440 Geochemistry 15, 1399–1416. https://doi.org/10.1016/S0883-2927(99)00118-3

441 Adachi, K., Kajino, M., Zaizen, Y., Igarashi, Y., 2013. Emission of spherical cesium-bearing particles
442 from an early stage of the Fukushima nuclear accident. Sci. Rep. 3, 2554.
443 https://doi.org/10.1038/srep02554

444 Braithwaite, J.W., 1980. Brine chemistry effects on the durability of a simulated nuclear waste glass, in:
445 Northrup, C.J.M. (Ed.), Scientific Basis for Nuclear Waste Management. Plenum Press, New York,
446 pp. 199–206.

447 Braun, K., Pochert, A., Beck, M., Fiedler, R., Gruber, J., Lindén, M., 2016. Dissolution kinetics of
448 mesoporous silica nanoparticles in different simulated body fluids. J. Sol-Gel Sci. Technol. 79,
449 319–327. https://doi.org/10.1007/s10971-016-4053-9

450 Buesseler, K., Dai, M., Aoyama, M., Benitez-Nelson, C., Charmasson, S., Higley, K., Maderich, V.,
451 Masqué, P., Morris, P.J., Oughton, D., Smith, J.N., 2017. Fukushima Daiichi–derived radionuclides
452 in the ocean: transport, fate, and impacts. Ann. Rev. Mar. Sci., Annual Review of Marine Science 9,
453 173–203. https://doi.org/10.1146/annurev-marine-010816-060733

454 Cabrini, M., Cigada, A., Rondell, G., Vicentini, B., 1997. Effect of different surface finishing and of
455 hydroxyapatite coatings on passive and corrosion current of Ti6Al4V alloy in simulated
456 physiological solution. Biomaterials 18, 783–787. https://doi.org/10.1016/S0142-9612(96)00205-0
457 Crovisier, J.L., Honnorez, J., Eberhart, J.P., 1987. Dissolution of basaltic glass in seawater: Mechanism
458 and rate. Geochim. Cosmochim. Acta 51, 2977–2990. https://doi.org/10.1016/0016-7037(87)90371-
459 1
460 Earle, S., 2015. Physical Geology, Creative C. ed. BC Open Campus Project.
461 Furuki, G., Imoto, J., Ochiai, A., Yamasaki, S., Nanba, K., Ohnuki, T., Grambow, B., Ewing, R.C.,
462 Utsunomiya, S., 2017. Caesium-rich micro-particles: A window into the meltdown events at the
463 Fukushima Daiichi Nuclear Power Plant. Sci. Rep. 7, 42731. https://doi.org/10.1038/srep42731
464 Gislason, S.R., Oelkers, E.H., 2003a. Mechanism, rates, and consequences of basaltic glass dissolution:
465 II. An experimental study of the dissolution rates of basaltic glass as a function of pH and
466 temperature. Geochim. Cosmochim. Acta 67, 3817–3832. https://doi.org/10.1016/S0016-
467 7037(03)00176-5
468 Gislason, S.R., Oelkers, E.H., 2003b. Mechanism, rates, and consequences of basaltic glass dissolution:
469 II. An experimental study of the dissolution rates of basaltic glass as a function of pH and
470 temperature. Geochim. Cosmochim. Acta 67, 3817–3832. https://doi.org/10.1016/S0016-
471 7037(03)00176-5

472 Grambow, B., 2011. Corrosion of Glass, in: Revie, R.W. (Ed.), Uhlig's Corrosion Handbook. John Wiley
473 & Sons, New Jersey, pp. 399–420.
474 Grambow, B., 1990. Chemistry of glass corrosion in high saline brines, in: Oversby, V.M., Brown, P.W.
475 (Eds.), Scientific Basis for Nuclear Waste Management. Plenum Press, Pittsburgh, PA, pp. 229–
476 240.
477 Hamilton, J.P., Pantano, C.G., Brantley, S.L., 2000. Dissolution of albite glass and crystal. Geochim.
478 Cosmochim. Acta 64, 2603–2615. https://doi.org/10.1016/S0016-7037(00)00388-4
479 Haynes, W.M., Lide, D.R., Bruno, T.J. (Eds.), 2014. CRC Handbook of Chemistry and Physics, 95th
480 Edition. CRC Press, Taylor & Francis Group, Boca Raton, FL.
481 Icenhower, J.P., Dove, P.M., 2000. The dissolution kinetics of amorphous silica into sodium chloride
482 solutions: effects of temperature and ionic strength. Geochim. Cosmochim. Acta 64, 4193–4203.
483 https://doi.org/10.1016/S0016-7037(00)00487-7
484 ICRP, 2012. Compendium of Dose Coefficients based on ICRP Publication 60. Ann. ICRP ICRP Publi.
485 ICRP, 1993. Age-dependent doses to members of the public from intake of radionuclides: Part 2.
486 Ingestion dose coefficients. Ann. ICRP 23, 1–167.
487 Ikehara, R., Suetake, M., Komiya, T., Furuki, G., Ochiai, A., Yamasaki, S., Bower, W.R., Law, G.T.W.,
488 Ohnuki, T., Grambow, B., Ewing, R.C., Utsunomiya, S., 2018. Novel Method of Quantifying
489 Radioactive Cesium-Rich Microparticles (CsMPs) in the Environment from the Fukushima Daiichi

Nuclear Power Plant. Environ. Sci. Technol. 52. https://doi.org/10.1021/acs.est.7b06693

Imoto, J., Furuki, G., Ochiai, A., Yamasaki, S., Nanba, K., Ohnuki, T., Grambow, B., Ewing, R.C., Utsunomiya, S., 2017a. Caesium fallout in Tokyo on 15th March, 2011 is dominated by highly radioactive, caesium-rich microparticles. Sci. Rep. In press. https://doi.org/10.1038/srep42118

Imoto, J., Ochiai, A., Furuki, G., Suetake, M., Ikehara, R., Horie, K., Takehara, M., Yamasaki, S., Nanba, K., Ohnuki, T., Law, G.T.W., Grambow, B., Ewing, R.C., Utsunomiya, S., 2017b. Isotopic signature and nano-texture of cesium-rich micro-particles: Release of uranium and fission products from the Fukushima Daiichi Nuclear Power Plant. Sci. Rep. 7, 5409. https://doi.org/10.1038/s41598-017-05910-z

Kaneko, M., Iwata, H., Shiotsu, H., Masaki, S., Kawamoto, Y., Yamasaki, S., Nakamatsu, Y., Imoto, J., Furuki, G., Ochiai, A., Nanba, K., Ohnuki, T., Ewing, R.C., Utsunomiya, S., 2015. Radioactive Cs in the Severely Contaminated Soils Near the Fukushima Daiichi Nuclear Power Plant. Front. Energy Res. 3, 37. https://doi.org/10.3389/fenrg.2015.00037

Ma, J., Huang, B.X., Zhao, X.C., Ban, C.L., Hao, X.H., Wang, C.Z., 2018. Substitutions of zinc in mesoporous silicate-based glasses and their physicochemical and biological properties. J. Non. Cryst. Solids 491, 98–105. https://doi.org/10.1016/J.JNONCRYSOL.2018.04.002

Marques, M.R.C., Loebenberg, R., Almukainzi, M., 2011. Simulated Biological Fluids with Possible Application in Dissolution Testing. Dissolution Technol. 18, 15–28.

508 https://doi.org/10.14227/DT180311P15

509 McMahon, P.B., Vroblesky, D.A., Bradley, P.M., Chapelle, F.H., Gullett, C.D., 1995. Evidence for

510 Enhanced Mineral Dissolution in Organic Acid-Rich Shallow Ground Water. Ground Water 33,

511 207–216. https://doi.org/10.1111/j.1745-6584.1995.tb00275.x

512 Ochiai, A., Imoto, J., Suetake, M., Komiya, T., Furuki, G., Ikehara, R., Yamasaki, S., Law, G.T.W.,

513 Ohnuki, T., Grambow, B., Ewing, R.C., Utsunomiya, S., 2018. Uranium Dioxides and Debris

514 Fragments Released to the Environment with Cesium-Rich Microparticles from the Fukushima

515 Daiichi Nuclear Power Plant. Environ. Sci. Technol. https://doi.org/10.1021/acs.est.7b06309

516 Oelkers, E.H., Gislason, S.R., 2001. The mechanism, rates and consequences of basaltic glass dissolution:

517 I. An experimental study of the dissolution rates of basaltic glass as a function of aqueous Al, Si

518 and oxalic acid concentration at 25°C and pH = 3 and 11. Geochim. Cosmochim. Acta 65, 3671–

519 3681. https://doi.org/10.1016/S0016-7037(01)00664-0

520 Ohtsuki, C., Kokubo, T., Yamamuro, T., 1992. Mechanism of apatite formation on CaOSiO2P2O5

521 glasses in a simulated body fluid. J. Non. Cryst. Solids 143, 84–92. https://doi.org/10.1016/S0022-

522 3093(05)80556-3

523 Okumura, T., Yamaguchi, N., Dohi, T., Iijima, K., Kogure, T., 2019. Dissolution behaviour of

524 radiocaesium-bearing microparticles released from the Fukushima nuclear plant. Sci. Rep. 9, 3520.

525 https://doi.org/10.1038/s41598-019-40423-x

526 Potter, R.., Mattson, S.M., 1991. Glass fiber dissolution in a physiological saline solution. Glas. Ber 64,
527 16–28.
528 Roy, M., 1989. Lung Clearance Modeling on the Basis of Physiological and Biological Parameters.
529 Health Phys. 57, 255–262. https://doi.org/10.1097/00004032-198907001-00033
530 Schlesinger, R.B., 1989. Deposition and clearance of inhaled particles., in: McClellan, R.O., Henderson,
531 R.F. (Eds.), Concepts in Inhalation Toxicology. Hemisphere, New York, pp. 163–192.
532 Scholze, H., 1991. Statement on chemical stability of silicate glass fibers. WaBoLu-Hefte.
533 Seidel, A., Löbbus, M., Vogelsberger, W., Sonnefeld, J., 1997. The kinetics of dissolution of silica
534 “Monospher” into water at different concentrations of background electrolyte. Solid State Ionics
535 101–103, 713–719. https://doi.org/10.1016/S0167-2738(97)00289-0
536 Stohl, A., Seibert, P., Wotawa, G., Arnold, D., Burkhart, J.F., Eckhardt, S., Tapia, C., Vargas, A.,
537 Yasunari, T.J., 2012. Xenon-133 and caesium-137 releases into the atmosphere from the Fukushima
538 Dai-ichi nuclear power plant: determination of the source term, atmospheric dispersion, and
539 deposition. Atmos. Chem. Phys. 12, 2313–2343. https://doi.org/10.5194/acp-12-2313-2012
540 Stumm, W., 1992. Chemistry of the Solid-Water Interface: Processes at the Mineral-Water Interface in
541 Natural Systems. John Wiley & Sons, Inc.
542 Tanaka, K., Sakaguchi, A., Kanai, Y., Tsuruta, H., Shinohara, A., Takahashi, Y., 2013. Heterogeneous
543 distribution of radiocesium in aerosols, soil and particulate matters emitted by the Fukushima

544 Daiichi Nuclear Power Plant accident: retention of micro-scale heterogeneity during the migration
545 of radiocesium from the air into ground and rive. J. Radioanal. Nucl. Chem. 295, 1927–1937.
546 https://doi.org/10.1007/s10967-012-2160-9
547 Vogelsberger, W., Löbbus, M., Sonnefeld, J., Seidel, A., 1999. The influence of ionic strength on the
548 dissolution process of silica. Colloids Surfaces A Physicochem. Eng. Asp. 159, 311–319.
549 https://doi.org/10.1016/S0927-7757(99)00268-X
550 Wen, C., Guan, S., Peng, L., Ren, C., Wang, X., Hu, Z., 2009. Characterization and degradation behavior
551 of AZ31 alloy surface modified by bone-like hydroxyapatite for implant applications. Appl. Surf.
552 Sci. 255, 6433–6438. https://doi.org/10.1016/j.apsusc.2008.09.078
553 Xiao, Y., Lasaga, A.C., 1994. Ab initio quantum mechanical studies of the kinetics and mechanisms of
554 silicate dissolution: H+(H3O+) catalysis. Geochim. Cosmochim. Acta 58, 5379–5400.
555 https://doi.org/10.1016/0016-7037(94)90237-2
556 Yamaguchi, N., Mitome, M., Kotone, A.-H., Asano, M., Adachi, K., Kogure, T., 2016. Internal structure
557 of cesium-bearing radioactive microparticles released from Fukushima nuclear power plant. Sci.
558 Rep. 6, 20548. https://doi.org/10.1038/srep20548
559 Yamasaki, S., Imoto, J., Furuki, G., Ochiai, A., Ohnuki, T., Sueki, K., Nanba, K., Ewing, R.C.,
560 Utsunomiya, S., 2016. Radioactive Cs in the estuary sediments near Fukushima Daiichi Nuclear
561 Power Plant. Sci. Total Environ. 551–552, 155–162. https://doi.org/10.1016/j.scitotenv.2016.01.155

562 **Figure captions**

563 **Fig. 1.** Scanning electron microscopy analysis of CsMPs used for dissolution experiments in the
564 present study. (a) Secondary-electron image of KOI CsMP associated with elemental maps. (b)
565 Secondary-electron image of OTZ CsMP and elemental maps.

566

567 **Fig. 2.** (a) A diagram showing the sequence of solutions used in the present dissolution experiment.
568 (b) A diagram illustrates the difference between two interval conditions: condition (i) and condition
569 (ii) during the interval for gamma measurement.

570

571

572 **Fig. 3.** Release of ^{137}Cs from KOI CsMP in various solutions (Seq. 1 – 5) as a function of time under
573 either wet and dry condition (i) or wet-only condition (ii). The CsMP was immersed in a sequence of
574 various solutions; simulated lung fluid at 25 ℃ under condition (i) (Seq. 1), ultrapure water at 25 ℃
575 under condition (i) (Seq. 2), simulated lung fluid at 37 ℃ under condition (i) (Seq. 3), artificial
576 seawater at 25 ℃ under condition (i) (Seq. 4), and simulated lung fluid at 25 ℃ under condition (ii)
577 (Seq. 5).

578

579 **Fig. 4.** Results of time course of ^{137}Cs radioactivity of KOI CsMP at 25 ℃ in various solutions under

wet and dry condition (i) or wet-only condition (ii) calculated based on ^{137}Cs release rate: (a) in SLF under condition (i); (b) in UPW under condition (i); (c) in ASW under condition (i); (d) in SLF under condition (ii). t_{100nm} and t_{total} represent the time required to reach 100 nm diameter and complete dissolution, respectively.

Fig. 5. Release of ^{137}Cs from OTZ CsMP in various solutions as a function of time under wet and dry condition (i). The CsMP was sequentially immersed in ultrapure water at 25 ℃ and simulated lung fluid at 25 ℃.

Fig. 6. Results of time course of ^{137}Cs radioactivity of OTZ CsMP at 25 ℃ in solutions under wet and dry condition (i) calculated based on ^{137}Cs release rate: (a) in UPW and (b) in SLF. t_{100nm} and t_{total} represent the time required to reach 100 nm diameter and complete dissolution, respectively. Note that the case for SLF solution (b) reveals the minimum period because the maximum release rate was used for calculation.

Fig. 7. (a) SEM image of OTZ before immersing in SLF associated with elemental maps of area indicated by red square. (b) SEM image of the same OTZ particle after ten days of immersion, with the elemental maps of the same area. (c) SEM-EDX spectrum of secondary precipitate indicated by

598 red square in panel (b).

599

600 **Fig. 8.** Schematic illustration of dissolution mechanisms for OTZ and KOI CsMPs. Illustration is based
601 on the inner texture of CsMPs with low and high Cs concentrations (Furuki et al., 2017; Imoto et al.,
602 2017a, 2017b).

603

604 **Fig. 9.** Comparison of dissolution rate calculated for OTZ with that of the other Si-based glasses
605 (Abraitis et al., 2000; Crovisier et al., 1987; Gislason and Oelkers, 2003b; Hamilton et al., 2000;
606 Icenhower and Dove, 2000; Oelkers and Gislason, 2001; Seidel et al., 1997) near room temperature.
607 As described in text, the rate for SLF at 25 °C is the maximum value and depicted by the arrow.

608

609 **Fig. 10.** Results of time course of Cs radioactivity for a potentially inhaled CsMP (2 μm in size) in
610 SLF under wet and dry condition (i) calculated assuming the maximum ^{137}Cs release rate of OTZ after
611 normalization by the composition. t_{100nm} and t_{total} represent the time required to reach 100 nm diameter
612 and complete dissolution, respectively.

613

614

615 Table 1. Radioactivity and associated parameters of CsMPs used for dissolution experiments.* The

616 radioactivity of Cs isotopes was decay-corrected to 15:36 on March 12, 2011. **Radioactivity per

617 unit mass was calculated assuming the spherical shape and a density of SiO_2 glass; 2.6 g/cm^3

618 (Haynes et al., 2014).

619

620

621

	Particle size (μm)	Radioactivity (Bq)		$^{134}Cs/^{137}Cs$ radioactivity ratio	$^{134+137}Cs$ Radioactivity per unit mass (Bq·g^{-1})**
		^{134}Cs	^{137}Cs		
OTZ	4.20	63.5 (±1.0)*	57.8 (±0.3)*	1.10	5.75×10^{11}
KOI	5.64	110 (±1)*	108 (±0)*	1.02	4.47×10^{11}

622

623

624

625

626

627 Table 2. ^{137}Cs radioactivity (Bq) released from CsMPs into various solutions as a function of time.

628 Errors are given in parentheses. The notation (i) indicates wet and dry condition and (ii) indicates

629 wet-only condition.

630

Duration	KOI					OTZ	
(day)	UPW	25°C SLF(i)	37°C SLF(i)	25°C SLF(ii)	ASW	UPW	SLF
1	1.18 (±0.02)	0.493 (±0.01)	0.259 (±0.006)	0.0585 (±0.0048)	0.0682 (±0.0069)	0.0235 (±0.0055)	0.0673 (±0.0060)
3	1.49 (±0.03)	0.660 (±0.02)	0.576 (±0.009)	0.0785 (±0.0048)	0.105 (±0.006)	0.0358 (±0.0043)	0.0937 (±0.0053)
10	1.59 (±0.02)	0.969 (±0.02)	1.03 (±0.02)	0.167 (±0.005)	0.168 (±0.005)	0.0501 (±0.0042)	0.129 (±0.006)
30	1.80 (±0.04)	-	1.49 (±0.03)	0.449 (±0.008)	0.400 (±0.009)	0.106 (±0.005)	-
31	-	1.79 (±0.04)	-	-	-	-	-
43	1.96 (±0.03)	-	-	-	-	-	-
63	-	-	1.91 (±0.04)		-	-	-

631

Table 3. Summary of ^{137}Cs release rate R_{Cs} from KOI and OTZ CsMPs at 25 °C. SLF (i) stands for immersion in SLF under condition (i) (wet and dry cycle). Condition (ii) is wet only. t_{total} and t_{100nm} are the time for the complete dissolution and the time to reach 100 nm diameter. *"n.a." in the table means that the data are not available. Note that the release rate from OTZ in SLF reveals the maximum value.

		SLF (i)	SLF (ii)	ASW	UPW
KOI	R_{Cs} ($\times 10^3$ Bq·m^{-2}·s^{-1})	4.68	1.54	1.29	1.33
	t_{total} (year)	19.1	58.1	69.5	67.6
	t_{100nm} (year)	18.5	56.0	67.0	65.2
OTZ	R_{Cs} ($\times 10^3$ Bq·m^{2}·s^{-1})	<1.04	n.a.*	n.a.*	0.549
	t_{total} (year)	>81.6	n.a.*	n.a.*	154
	t_{100nm} (year)	>77.7	n.a.*	n.a.*	147

Figure

Click here to download Figure: Suetake2019Chemosphere revision 1 Figure.pdf

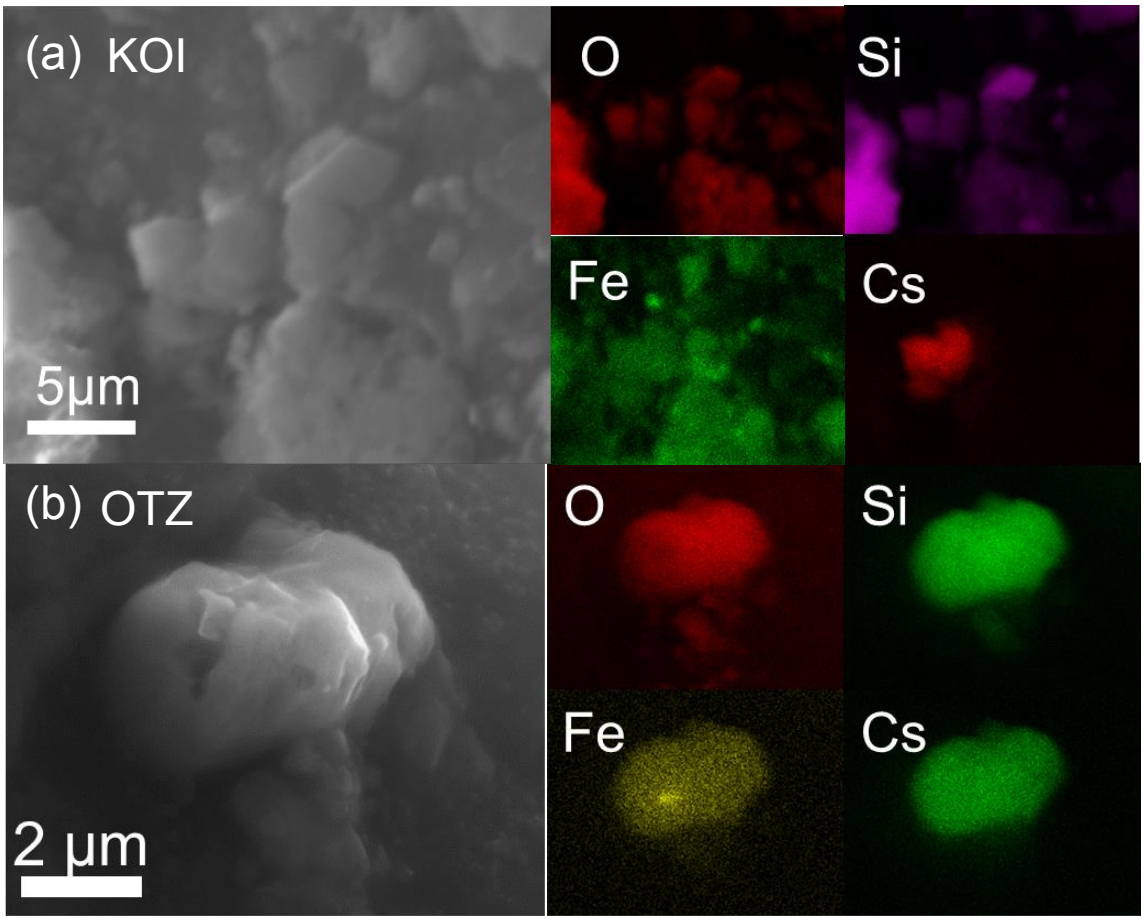

Fig. 1

(a)

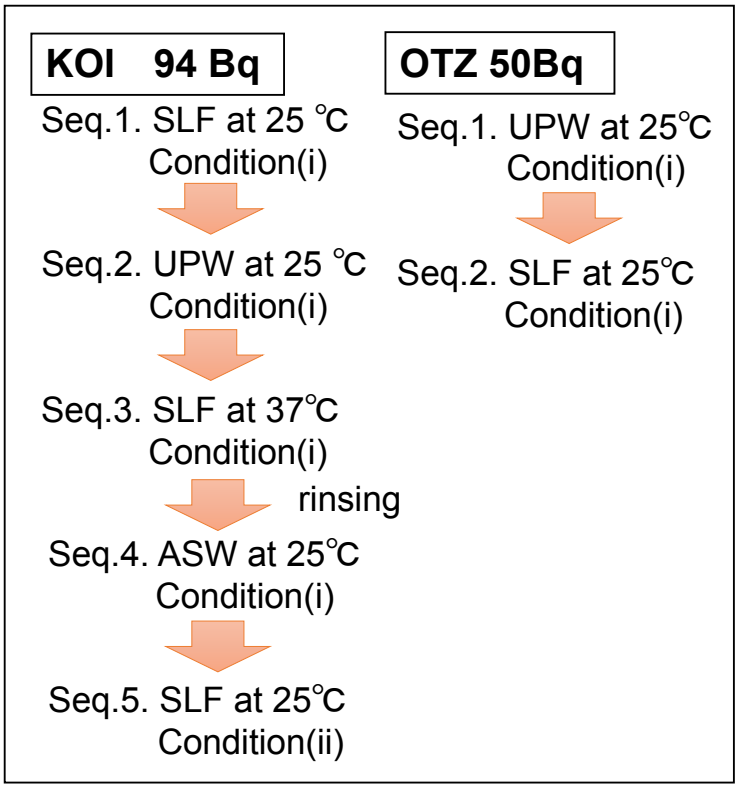
KOI 94 Bq
Seq.1. SLF at 25 ℃
Condition(i)
Seq.2. UPW at 25 ℃
Condition(i)
Seq.3. SLF at 37℃
Condition(i)
rinsing
Seq.4. ASW at 25℃
Condition(i)
Seq.5. SLF at 25℃
Condition(ii)
OTZ 50Bq
Seq.1. UPW at 25℃
Condition(i)
Seq.2. SLF at 25℃
Condition(i)

(b)

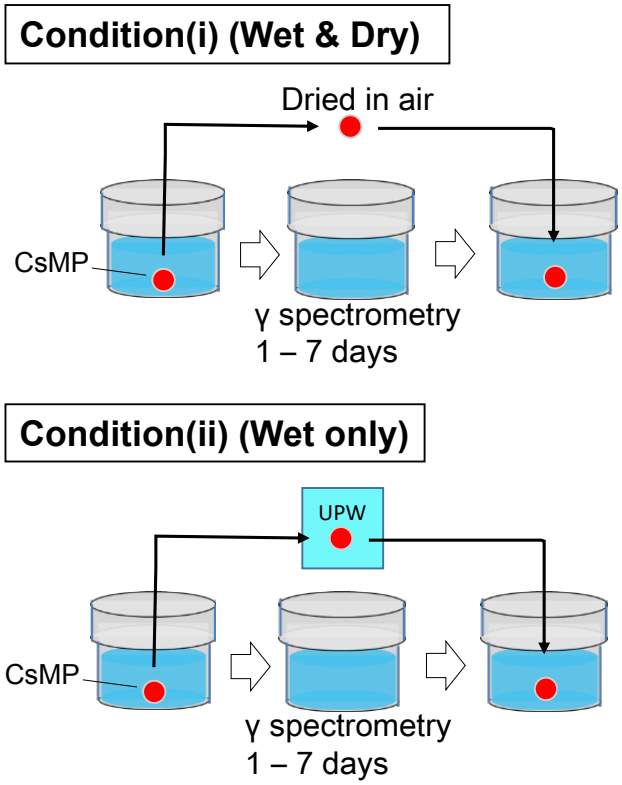
Condition(i) (Wet & Dry)
Dried in air
CsMP
γ spectrometry
1 – 7 days
Condition(ii) (Wet only)
UPW
CsMP
γ spectrometry
1 – 7 days

Fig. 2

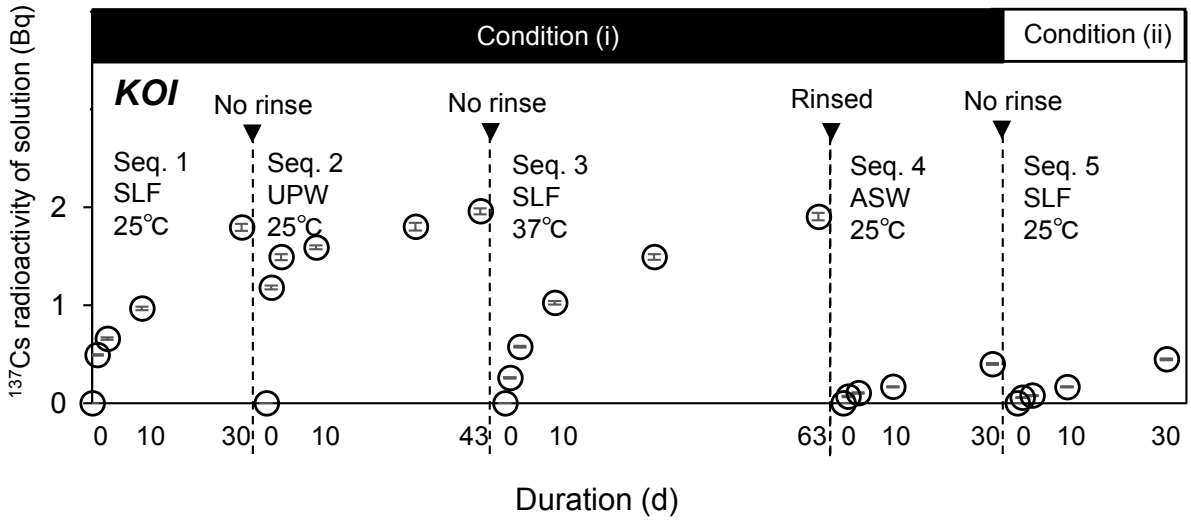
Condition (i)
Condition (ii)
KOI
No rinse
No rinse
Rinsed
No rinse
Seq. 1
SLF
25℃
Seq. 2
UPW
25℃
Seq. 3
SLF
37℃
Seq. 4
ASW
25℃
Seq. 5
SLF
25℃
137Cs radioactivity of solution (Bq)
0
1
2
0 10 30 0 10 43 0 10 63 0 10 30 0 10 30
Duration (d)

Fig. 3

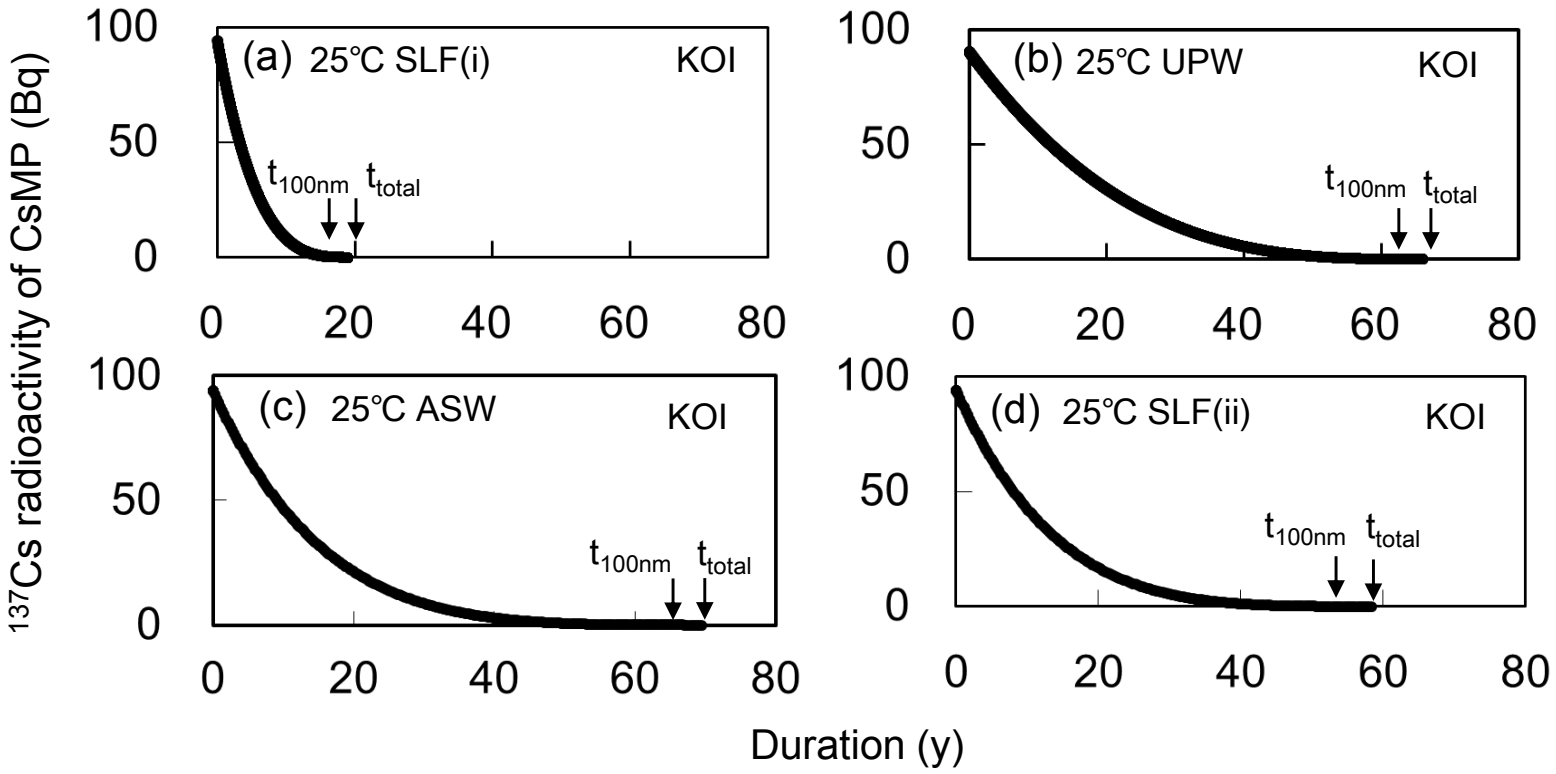
(a) 25℃ SLF(i)
KOI
(b) 25℃ UPW
KOI
(c) 25℃ ASW
KOI
(d) 25℃ SLF(ii)
KOI
t_{100nm}
t_{total}
100
50
0
0
20
40
60
80
^{137}Cs radioactivity of CsMP (Bq)
Duration (y)

Fig. 4

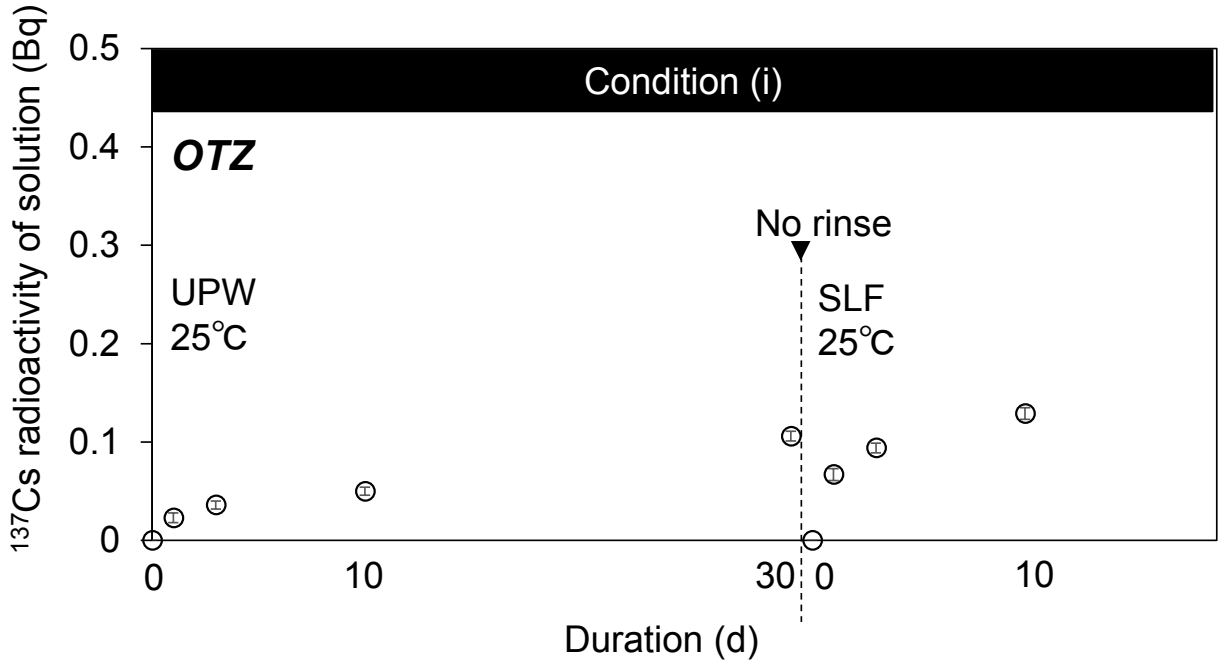
Condition (i)
OTZ
No rinse
UPW
25℃
SLF
25℃
137Cs radioactivity of solution (Bq)
0.5
0.4
0.3
0.2
0.1
0
0
10
30
0
10
Duration (d)

Fig. 5

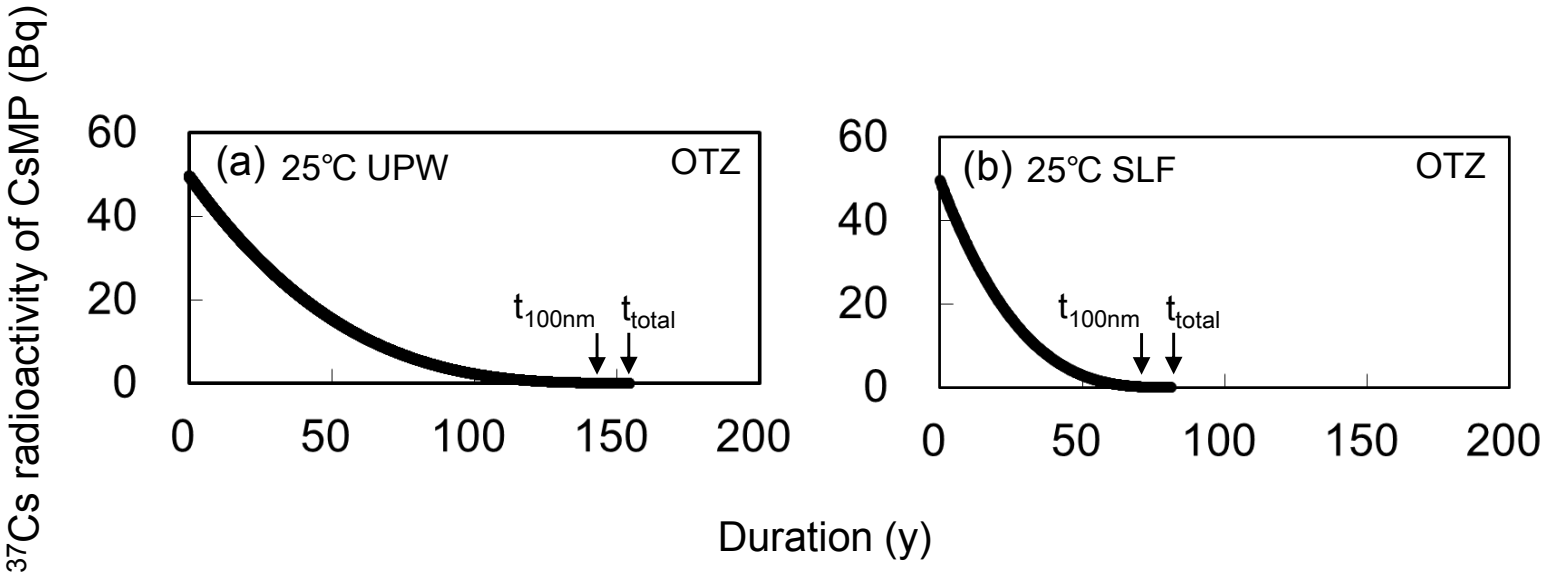
137Cs radioactivity of CsMP (Bq)
60
40
20
0
(a) 25℃ UPW
OTZ
t100nm
ttotal
0
50
100
150
200
(b) 25℃ SLF
OTZ
Duration (y)

Fig. 6

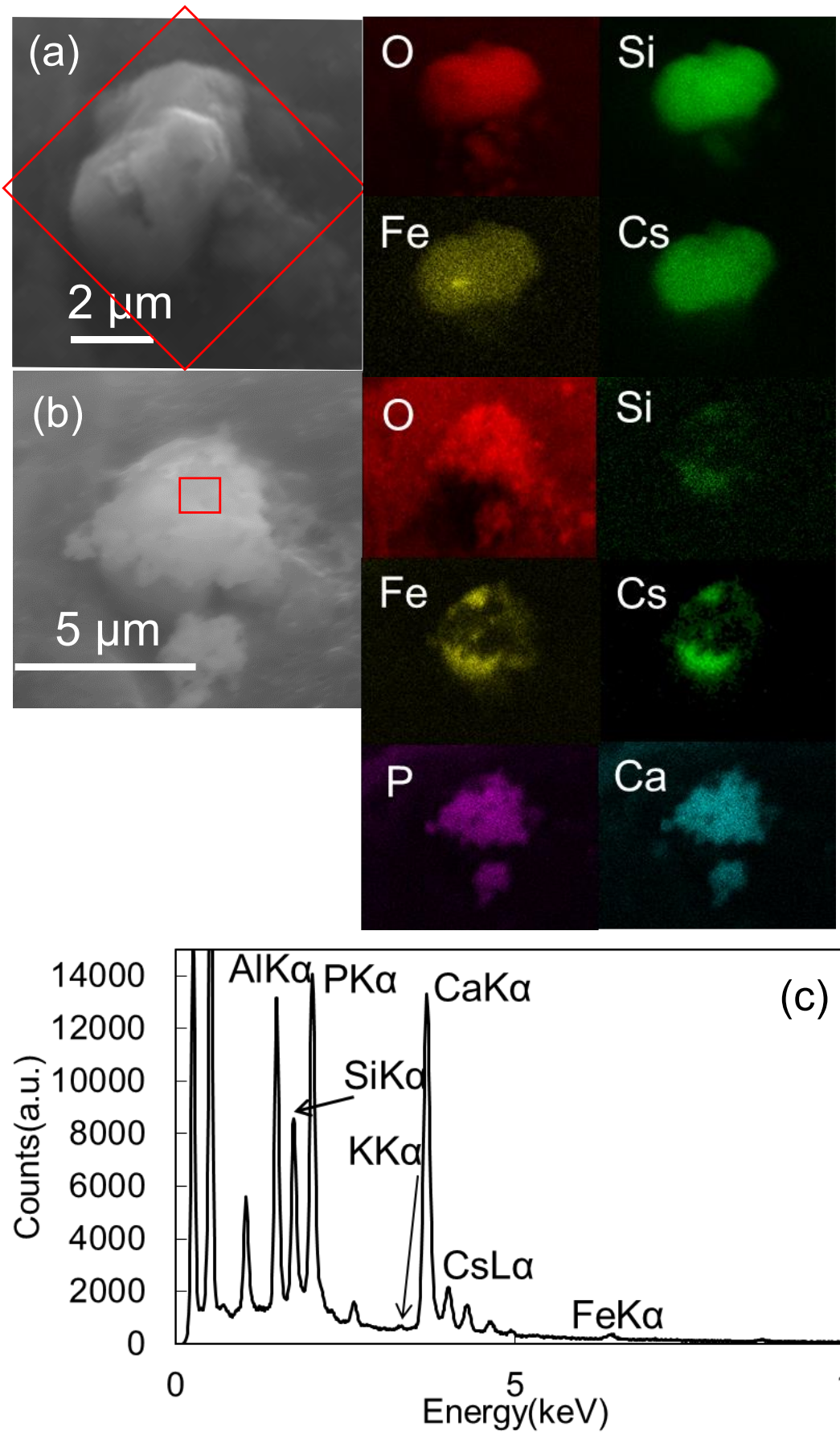
(a)
2 μm
O
Si
Fe
Cs
(b)
5 μm
O
Si
Fe
Cs
P
Ca
(c)
AlKα
PKα
CaKα
SiKα
KKα
CsLα
FeKα
Counts(a.u.)
14000
12000
10000
8000
6000
4000
2000
0
0
5
10
Energy(keV)

Fig. 7

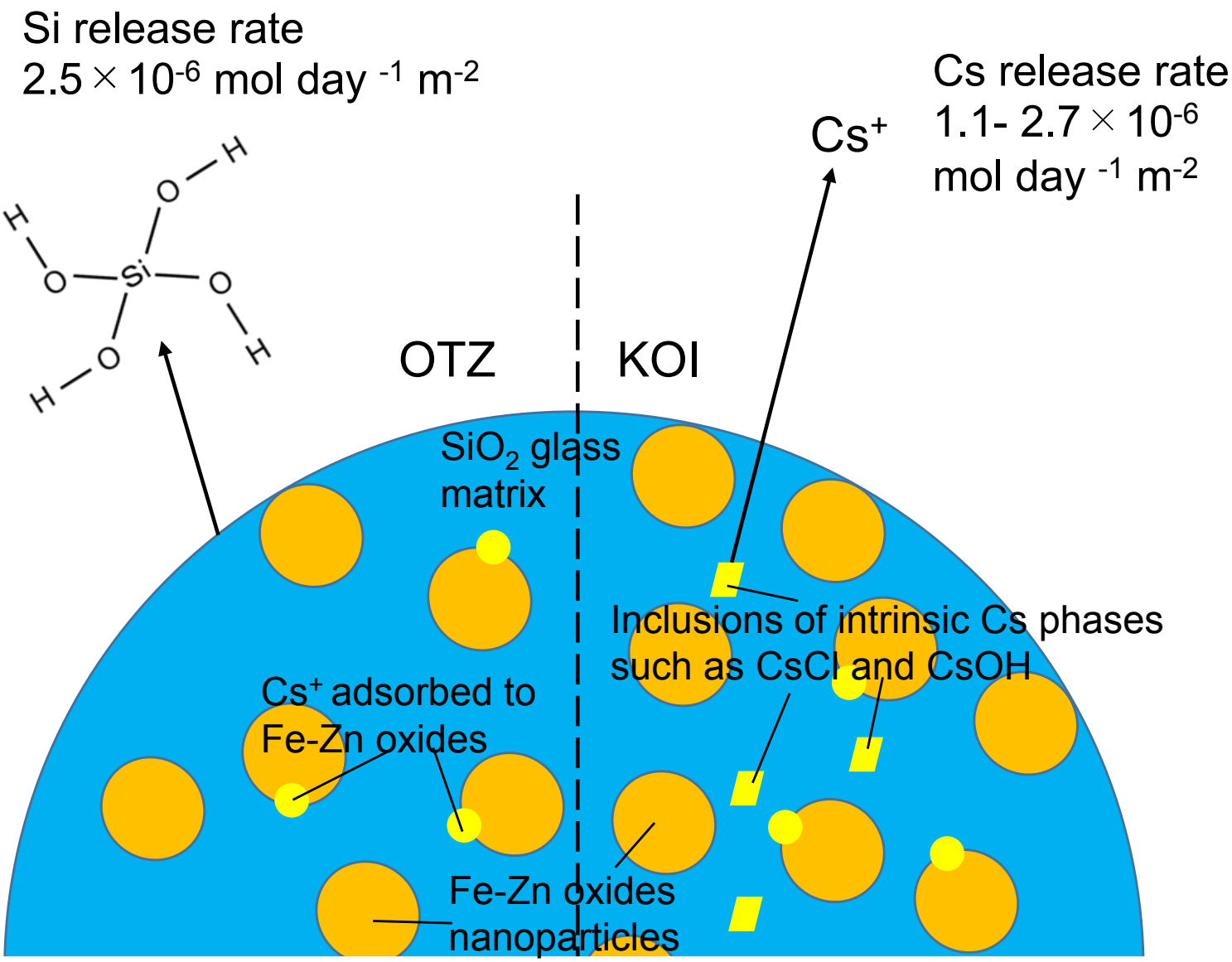
Si release rate
2.5 × 10-6 mol day -1 m-2
Cs release rate
1.1- 2.7 × 10-6
mol day -1 m-2
Cs+
OTZ
KOI
SiO2 glass
matrix
Inclusions of intrinsic Cs phases
such as CsCl and CsOH
Cs+ adsorbed to
Fe-Zn oxides
Fe-Zn oxides
nanoparticles

Fig. 8

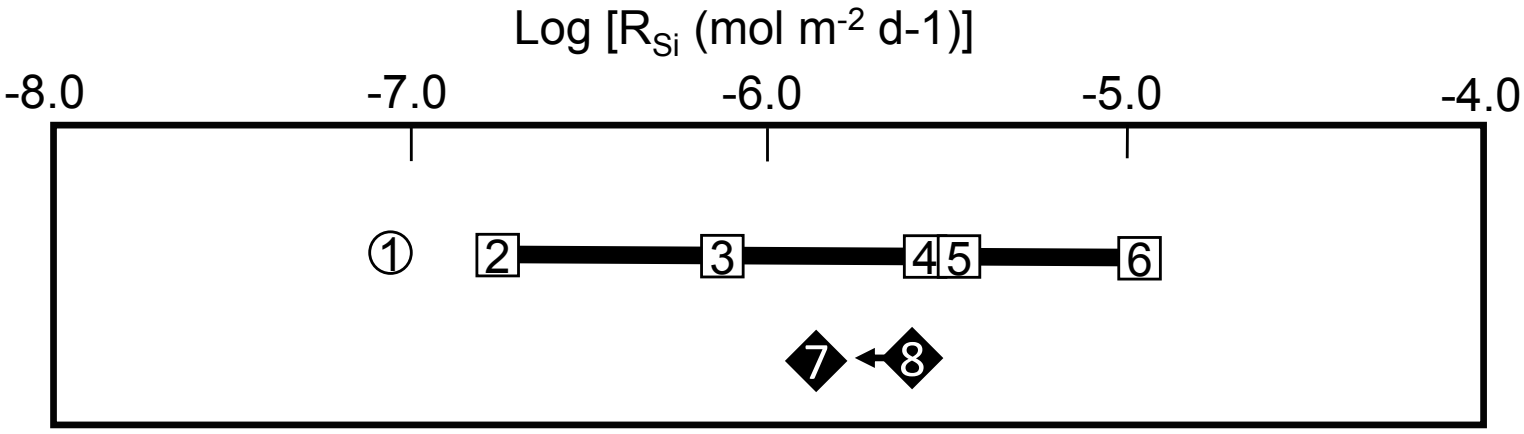

① Amorphous silica; 25 ℃ in deionized water (Seidel et al., 1997; Icenhower and Dove, 2000)

Si-based glass

- 2 SiO_2:68.6%; 25 ℃; deionized water; pH 5.6 (Hamilton et al., 2000)
- 3 SiO_2: 47.5% B_2O_3:16.9% ;18 ℃, Tris(hydroxymethyl)-Methylamine,HNO_3,KOH; pH 7 (Abraitis et al., 2000)
- 4 SiO_2: 48.1%; 25 ℃; HCl, NaOH,$C_2H_2O_4$; pH 7 (Oelker and Gislason., 2001)
- 5 SiO_2: 49.8%; 29 ℃; HCl, NH_4Cl, and NH_3; pH 7.0 (Gislason and Oelker, 2003)
- 6 SiO_2: 50.76%; 25 ℃; seawater; pH 8.0 (Crovisier et al., 1987)

7 OTZ; 25 ℃; SiO_2: 65.1%; UPW; pH 7 (This study)

8 OTZ; 25 ℃; SiO_2: 65.1%; SLF; pH 7.4 (This study)

Fig. 9

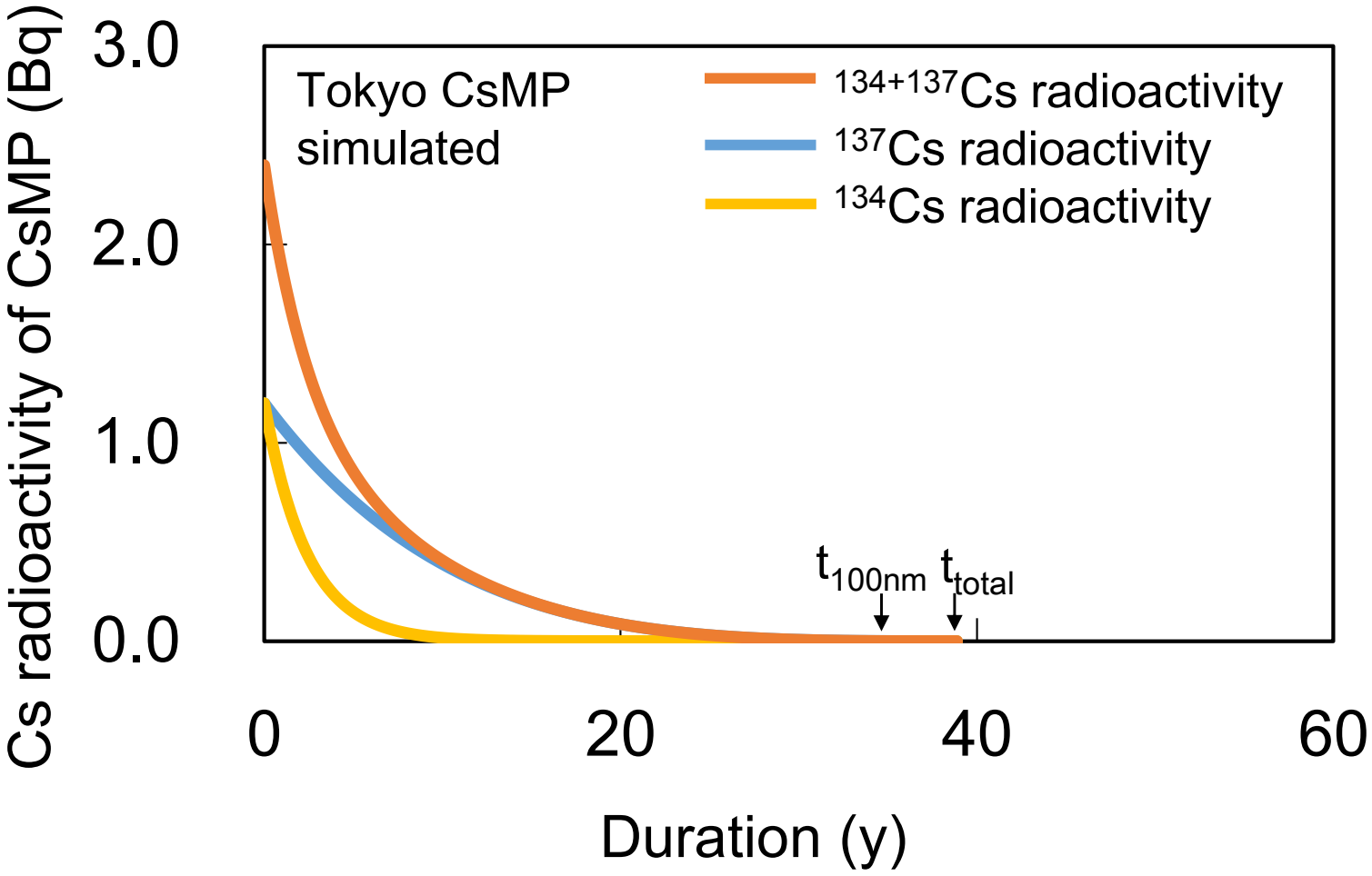
Tokyo CsMP
simulated
134+137Cs radioactivity
137Cs radioactivity
134Cs radioactivity
t100nm
ttotal
Cs radioactivity of CsMP (Bq)
3.0
2.0
1.0
0.0
0
20
40
60
Duration (y)

Fig. 10

Supplementary Material

Click here to download Supplementary Material: Suetake2019Chemosphere revision 1 Supplementary Materials.pdf